

## HOW TO COADD IMAGES? II. A COADDITION IMAGE THAT IS OPTIMAL FOR ANY PURPOSE IN THE BACKGROUND DOMINATED NOISE LIMIT

BARAK ZACKAY<sup>1</sup> AND ERAN O. OFEK<sup>1</sup>

*Submitted to ApJ*

### ABSTRACT

Image coaddition is one of the most basic operations that astronomers perform. In Paper I, we presented the optimal ways to coadd images in order to detect faint sources and to perform flux measurements under the assumption that the noise is approximately Gaussian. Here, we build on these results and derive from first principles a coaddition technique which is optimal for any hypothesis testing and measurement (e.g., source detection, flux or shape measurements and star/galaxy separation), in the background-noise-dominated case. This method has several important properties. The pixels of the resulting coadd image are uncorrelated. This image preserves all the information (from the original individual images) on all spatial frequencies. Any hypothesis testing or measurement that can be done on all the individual images simultaneously, can be done on the coadded image without any loss of information. The PSF of this image is typically as narrow, or narrower than the PSF of the best image in the ensemble. Moreover, this image is practically indistinguishable from a regular single image, meaning that any code that measures any property on a regular astronomical image can be applied to it unchanged. In particular, the optimal source detection statistic derived in paper I is reproduced by matched filtering this image with its own PSF. This coaddition process, which we call proper coaddition, can be understood as a the maximum signal-to-noise ratio measurement of the Fourier transform of the image, weighted in such a way that the noise in the entire Fourier domain is of equal variance. This method has important implications for multi-epoch seeing-limited deep surveys, weak lensing galaxy shape measurements, and diffraction-limited imaging via speckle observations. The last topic will be covered in depth in future papers. We provide an implementation of this algorithm in MATLAB.

*Subject headings:* techniques: image processing — techniques: photometric

### 1. INTRODUCTION

Practically all ground-based surveys are subject to the ever-changing atmospheric seeing conditions, sky brightness and transparency. These changes produce large variations in both resolution and depth of astronomical observations. It is often necessary to image the same area of sky repeatedly, in order to both increase survey depth, and to allow time-dependent science cases. Examples for such surveys are LSST (Ivezic et al. 2008), DES (The Dark Energy Survey Collaboration 2005), PTF (Law et al. 2009), CFHTLS (Hoekstra et al. 2006), Pan-STARRS (Kaiser et al. 2002), SkyMapper (Keller et al. 2007) and SDSS (York et al. 2000).

In order to simultaneously pursue all science cases that require coaddition, there is a demand for a method that preserves all the information that exists in the data in one coadded image, leaving the original data redundant. Putting this in formal language, we would like to construct an image which is a sufficient statistic<sup>2</sup> for any further processing of the data, such as source detection, applying shear measurements or performing astrometric measurements.

It is non-trivial that such an image exists, as currently no coaddition technique is used for all purposes and existing methods fail to encompass all the data. For example, for many applications it is customary to use only images with favorable seeing. In some cases (e.g., lucky imaging; Law et al. 2006) it is common to discard  $> 90\%$  of the data. Even for the simple purpose of maximal sensitivity for source detection, various

authors use different weighing schemes for the image combination (e.g., Annis et al. 2014; Jiang et al. 2014).

This paper is number II in a series of papers on the problem of image coaddition. In paper I (Zackay & Ofek 2015) we presented the best way to coadd images for source detection and flux measurement under several different regimes of noise properties. In this paper, we focus on the background-noise-dominated regime and describe a coaddition method that is optimal for performing any measurement or hypotheses testing on the data (for non-variable sources). The product of this coaddition method is therefore a sufficient statistic for any further processing. We note that the background dominated noise limit is the most common case in astronomical observations.

We show that the coadded image also has an intuitive explanation as being the best “proper” image, where we define an image being proper if its additive noise component satisfies that *i*) All pixels have equal variance and *ii*) All pairs of pixels are uncorrelated. We also show that this image behaves exactly like an ordinary image, which means that any single-image analysis code that exists will operate correctly on it, exploiting all the information that existed in the original dataset.

After completing the work on this paper, we became aware that a similar method to the one we derive was already presented in Homrighausen et al. (2011) without any formal derivation. They refer to this method, as well as another deconvolution method, as a private communication from N. Kaiser (2004). Homrighausen et al. (2011) mention that this method has some associated optimality properties, but they argue that the gain from using this method is marginal. Here we show that the method presented in this paper is the optimal way to coadd a stack of images in the background-dominated-

<sup>1</sup> Department of Particle Physics and Astrophysics, Weizmann Institute of Science, 76100 Rehovot, Israel

<sup>2</sup> A statistic is sufficient with respect to a model and its associated parameter if no other statistic that can be calculated from the same sample provides any additional information as to the value of the models parameter.

noise limit, and a sufficient statistic for any further signal processing. Tested on real data, we demonstrate that for seeing-limited surveys this method provide a few percents to 25% increase in survey speed compared with weighted coaddition schemes (e.g., Annis et al. 2014; Jiang et al. 2014). Furthermore, we claim that usage of this method may have additional far-reaching consequences, as we show in this and future papers. Homrighausen et al. (2011) further argue that this method is a biased estimator of the *true* image and that another method - namely the deconvolution method, although numerically unstable, has the smallest variance of all methods. It is worth while to analyze these statements as they may help us understand the apparent conflict between our results and those of Homrighausen et al. (2011). In practice a reconstruction of the true image is impossible (unless the  $S/N$  is infinite and the PSF is known exactly) as in general our knowledge of the spatial high frequencies is greatly suppressed by the PSF. Therefore, the desired property from a coaddition method is not to reconstruct the true image, but rather to provide a sufficient statistic representing all the observed data in one image. This allows us to test hypotheses and to measure properties of sources in the true image, in an unbiased way and with the highest precision. The metrics which Homrighausen et al. (2011) apply to compare different image coaddition techniques are image quality metrics like the PSF width and the mean integrated squared error of the image from the true scene. These metrics do not represent accurately the requirement for maximal sensitivity of measurements made using the coadded image. These are the major differences between the approach taken by Homrighausen et al. (2011) and our methodology.

The structure of the paper is as follows: In §2 we present the statistical model and assumptions. In §3 we present an intuitive definition of what is a natural astronomical image, which we call a *proper image*. In §4 we convert the optimal source detection statistic presented in Zackay & Ofek (2015) to a proper image. In §5 we show that the derived image is a sufficient statistic for any statistical test or decision based on the data. In §6 we show examples of the application of the proper image coaddition statistic to both simulated PSFs and real data. In §7 we discuss the implementation details relevant to the successful application of the coaddition method. In §8 we highlight the key results and equations, and discuss the implications of this coaddition method to future surveys.

## 2. STATISTICAL FORMALISM

Following the same notation as in paper I, we denote the  $j$ 'th background subtracted image, in a series of observations of the same position, by  $M_j$ . All the images are assumed to be registered. This image can be described by the convolution of the true, background subtracted, noiseless image  $T$  with the image point spread function (PSF)  $P_j$ , added to which is a noise term  $\epsilon_j$ ,

$$M_j = (F_j T) \otimes P_j + \epsilon_j, \quad (1)$$

where  $F_j$  is a multiplicative factor that describes the transparency<sup>3</sup> and  $\otimes$  represents convolution. The noise term  $\epsilon_j$  has a variance:

$$V[\epsilon_j] = B_j + (F_j T) \otimes P_j, \quad (2)$$

<sup>3</sup> More accurately, the product of transparency, exposure time, effective collecting area of the optical system and the detector efficiency.

where  $B_j$  is the image background (or more generally, the total variance that is homogeneous across the image – i.e., including the read noise). Here, for simplicity, we assume that the image gain is 1, and that the background noise is the dominant source of noise, i.e

$$(F_j T) \otimes P_j \ll B_j. \quad (3)$$

Using this, we can write

$$V[\epsilon_j] \equiv \sigma_j^2 \approx B_j. \quad (4)$$

We further assume that the Poisson noise of the background to be Gaussian with good approximation (e.g.,  $B_j \gtrsim 30$ ), and that the noise component in different pixels is uncorrelated.

Equation 4 holds in many astronomical images. Given typical ground-based visible-light sky-background value (e.g.,  $m_{\text{sky}} \sim 18 - 21 \text{ mag arcsec}^{-2}$ ) and typical fraction of an arcsecond pixel size. This means that this condition is satisfied for all objects with surface brightness fainter than about  $21 \text{ mag arcsec}^{-2}$ .

### 2.1. Coadding images for source detection

In paper I we presented the best coadded image for source detection under the assumption that the noise in all observations is (locally) spatially homogeneous, Gaussian, and that the noise component of different pixels is uncorrelated. This image is given by:

$$S = \sum_j \left( \frac{F_j \overleftarrow{P}_j}{\sigma_j^2} \right) \otimes M_j, \quad (5)$$

where  $\overleftarrow{P}_j(x, y) = P_j(-x, -y)$ .

This image is essentially the equivalent of a matched filtered image for an ensemble of images. Therefore  $S$  is a score image, showing the log-likelihood for the existence of a source in each position. Matched-filtered images, while being best for source detection, are not sharp because they have an effective PSF which is twice the one of the original image. This is the reason that albeit optimal for source detection, astronomers usually do not look at matched-filtered images. Furthermore, matched-filtered images cannot be intuitively interpreted for any purpose other than single source detection because neighboring pixels of these images are highly correlated. For example, performing galaxy shape measurements requires the spatial covariance matrix.

## 3. NOISE PROPERTIES OF IMAGES, AND THE DEFINITION OF A PROPER IMAGE

A major difference between the coaddition product described in Equation 5 and a regular astronomical observation, is that the noise in neighboring pixels of  $S$  is highly correlated due to the matched-filtering operation. The correlated noise properties of matched-filtered images requires special care whenever we perform any statistical test or measurement. For example, fitting a model (e.g., a galaxy shape model) to a light source, in an image with correlated noise, requires considerable effort in diagonalizing the covariance matrix of the many pixels involved. This motivates us to define a *proper image* to be an image that satisfies the following two conditions:

I All the pixels in the additive noise component have equal variance<sup>4</sup>.

<sup>4</sup> Practically, the equal variance assumption can be relaxed to the assump-

II Different pixels of the additive noise component ( $\varepsilon_j$ ) are uncorrelated.

Since in most (background subtracted) astronomical images the noise can be assumed to be approximately Gaussian, Conditions I and II imply that all pixels will be independent and identically distributed (i.i.d.). A property of proper images is that the Fourier transform of its noise component also satisfies conditions I and II. The converse is also true, if the Fourier transform of an image satisfies conditions I and II, the image itself is proper.

We note that any linear combination of images that are directly measured from the telescope, is (at least locally) a proper image. A few examples of non-proper images:

- A matched-filtered image is not proper, since the noise in neighboring pixels is correlated.
- A deconvolved image is not proper, as long range correlations are always present in images that are the product of deconvolution.
- A proper image that has been “flat fielded” is no longer a proper image. The reason is that the variance of such images is position dependent. However, if the flat field is sufficiently smooth, it could be approximately regarded as proper because as we will show, all the operations done on proper coadd images are local operations.
- An image with a strong source, that either saturates the detector, or is much brighter than the sky background is not proper. Note that any slice of this image that does not contain significant contamination from the bright source can be regarded as a proper image.

#### 4. THE BEST PROPER IMAGE

There are many ways to coadd proper images and to produce a new (coadded) proper image. However, we are interested in a proper image which maximizes the signal to noise ratio ( $S/N$ ) of the faintest sources. Such an image must preserve the depth of the original set of images. Moreover we would like our image to preserve all spatial information, which could be interpreted as having the best possible  $S/N$  in each spatial frequency. As we will show below, these two requirements coincide. The best starting point for such an image is to start by turning the statistic  $S$  (Eq. 5), which is optimal for source detection, into a proper image. In order to make a proper image from the statistic  $S$ , we examine its Fourier transform:

$$\widehat{S}(f) = \sum_j \frac{F_j}{\sigma_j^2} \overline{\widehat{P}_j(f)} \widehat{M}_j(f). \quad (6)$$

Here,  $f = (f_1, f_2)$  is the spatial frequency (two dimensional) index, and we will omit it from now on. The hat sign  $\widehat{\phantom{x}}$  represents Fourier transform, while the accent  $\overline{\phantom{x}}$  marks complex conjugation. When the overline accent appears above the hat symbol it means that the complex conjugate follows the Fourier transform.

The additive noise frequencies in  $\widehat{S}$  are uncorrelated. They were uncorrelated in each of the Fourier transformed original

tion of a background which is not a strong function of spatial position. This is because all operations we apply are effectively local, and the image at a certain pixel involves only weighted summation of pixels which are up to a few PSF widths of the original position in all images.

images  $\widehat{M}_j$ , and therefore are uncorrelated after their weighted addition. Furthermore, the frequencies of  $\widehat{M}_j$  have equal variance as we assumed the images  $\widehat{M}_j$  are proper (this happens whenever the source noise is negligible). However, the frequencies of the product  $\widehat{P}_j \widehat{M}_j$  are not of equal variance, as  $|\widehat{P}_j|$  can change drastically between low and high frequencies. In order to transform this image into a proper image, all we need to do is to normalize each frequency by its own standard deviation. Calculating the standard deviation of each pixel, we can get the Fourier transform of the proper image:

$$\widehat{R} = \frac{\sum_j \frac{F_j}{\sigma_j^2} \overline{\widehat{P}_j} \widehat{M}_j}{\sqrt{\sum_j \frac{F_j^2}{\sigma_j^2} |\widehat{P}_j|^2}}. \quad (7)$$

The noise in  $\widehat{R}$  satisfies conditions I and II, and hence, its inverse Fourier transform  $R$  is also a proper image.

The reason that  $R$  preserves all spatial information, is because in the computation of each frequency of  $\widehat{R}$ , we add random variables scaled by their (conjugate) expectation, divided by the variance. We can identify this operation as the maximal  $S/N$  addition of random variables, shown in the Appendix of paper I. This means that each of the frequencies of  $\widehat{R}$  is the maximum  $S/N$  linear estimator of  $\widehat{T}$ , where each frequency is scaled to have the same noise variance. Therefore,  $R$  is not just a proper image, it is the optimal proper image in the limit of background dominated noise.

Interestingly, as  $R$  is a proper image, and behaves like a standard image, a natural question is therefore what is its PSF? The PSF of an image is the normalized response of the image to a point-source located at position  $(0,0)$ , i.e., when  $T = \delta_{(0,0)}$ ,  $\varepsilon_j = 0$ , (where  $\delta_{(0,0)}$  denotes an image with one at the origin and zero otherwise) which means  $\widehat{T} = 1$ ,  $\widehat{\varepsilon}_j = 0$ . For example, by evaluating  $\widehat{M}_j$  with these substitutions, we get  $\widehat{P}_j$ :

$$\widehat{M}_j = F_j \widehat{T} \widehat{P}_j + \widehat{\varepsilon}_j = F_j \widehat{P}_j \propto \widehat{P}_j. \quad (8)$$

Repeating this process for  $R$ , by substituting Equation 8 into Equation 7 we get the Fourier transform of the PSF of the proper coaddition image, which we denote by  $P_R$ :

$$\widehat{P}_R \propto \frac{\sum_j \frac{F_j}{\sigma_j^2} \overline{\widehat{P}_j} F_j \widehat{P}_j}{\sqrt{\sum_j \frac{F_j^2}{\sigma_j^2} |\widehat{P}_j|^2}} = \sqrt{\sum_j \frac{F_j^2}{\sigma_j^2} |\widehat{P}_j|^2}. \quad (9)$$

Normalizing  $P_R$  to have unit sum, we get:

$$\widehat{P}_R = \frac{\sqrt{\sum_j \frac{F_j^2}{\sigma_j^2} |\widehat{P}_j|^2}}{\sqrt{\sum_j \frac{F_j^2}{\sigma_j^2} |\widehat{P}_j|^2}} \equiv \frac{\sqrt{\sum_j \frac{F_j^2}{\sigma_j^2} |\widehat{P}_j|^2}}{F_R}, \quad (10)$$

where  $F_R$  is the equivalent of transparency for the properly coadded image. The standard deviation of the properly coadded image (Eq. 7),  $\sigma_R$ , is given by:

$$\sigma_R = 1, \quad (11)$$

Finally, we can express the full statistical model for the coadded image  $R$  by:

$$R = F_R T \otimes P_R + \varepsilon_R, \quad (12)$$

where  $\varepsilon_R$  are uncorrelated Gaussian variables with

$$V[\varepsilon_R] = \sigma_R^2 = 1. \quad (13)$$

Not surprisingly, the log-likelihood ratio for the existence of a point source in the coadded image, defined in Equation 5,  $S$ , can be computed by matched-filtering  $R$  with its PSF:

$$S = \frac{F_R}{\sigma_R^2} \overleftarrow{P}_R \otimes R. \quad (14)$$

Equivalently, in fourier space:

$$\widehat{S} = \frac{F_R}{\sigma_R^2} \overleftarrow{P}_R \widehat{R}. \quad (15)$$

Therefore, for source detection, this method is identical to the technique presented in paper I.

An important remark is that  $P_R$  is numerically stable. In contrast with deconvolution that is often suggested for coaddition, there is no division by small numbers in the process of calculating  $R$  and  $P_R$ . This is evident from the fact that every effective kernel of every measurement  $M_j$  in the numerator of Equation 7 is proportional to  $|P_j|$ , while the denominator is larger than  $|P_j|$  (triangle inequality). Hence, in the limit of  $P_j \rightarrow 0$  Equation 7 will not diverge.

A demonstration of the properly coadded images that we get when adding several sets of simulated examples are shown in Figure 1 (see §6).

### 5. $R, P_R$ ARE SUFFICIENT FOR ANY FURTHER PROCESSING

Although having an image that you can intuitively understand is useful, the importance of the best proper image does not end here. In this section, it is our goal to show that any scientific question about the data (e.g., galaxy shapes), which is not time variable, can be answered using the proper image, without any further necessity to access or even store the original data. In §5.1 we will show that  $R$  and  $P_R$  are sufficient for a statistical decision between any two generative hypotheses, meaning that using these will not result in any information loss with respect to performing the hypothesis testing using the entire set of images simultaneously. In §5.2 we will extend this result to the case of performing any measurement (e.g., photometry, astrometry and shape measurements).

#### 5.1. $R, P_R$ are sufficient for any hypothesis testing task

Assuming that we want to decide between two generative models for  $T$ . In the case of the first (null) hypothesis  $\mathcal{H}_0$ , our model for the truth image is  $T_0$ , and in the case of the second hypothesis  $\mathcal{H}_1$ , our model for the truth image is  $T_1$ . Given  $\mathcal{H}_0$ , the images are of the form:

$$M_j = (F_j T_0) \otimes P_j + \varepsilon_j, \quad (16)$$

and given  $\mathcal{H}_1$ , the images are of the form:

$$M_j = (F_j T_1) \otimes P_j + \varepsilon_j. \quad (17)$$

Rearranging Equation 16, and noting that convolution with a delta function ( $\delta_{(0,0)}$ ) returns a constant, we get:

$$M_j = (F_j T_0) \otimes P_j + \varepsilon_j = (\delta_{(0,0)} F_j) \otimes (T_0 \otimes P_j) + \varepsilon_j, \quad (18)$$

For convenience, we will add a reference hypothesis,  $\mathcal{H}_2$  of the form (i.e., no sources)

$$M_j = \varepsilon_j. \quad (19)$$

Applying our solution from paper I for the point source detection problem, we can calculate the log likelihood ratio<sup>5</sup> between hypothesis  $\mathcal{H}_\alpha$  and  $\mathcal{H}_2$ , where  $\alpha \in \{0, 1\}$ .

$$\mathcal{L}_{\alpha,2} = \ln(\mathcal{P}[M|\mathcal{H}_\alpha]) - \ln(\mathcal{P}[M|\mathcal{H}_2]), \quad (20)$$

where  $\mathcal{P}[M|\mathcal{H}_\alpha]$  denotes the probability to observe  $M$  given the hypothesis  $\mathcal{H}_\alpha$  is true. In paper I we showed that this log likelihood ratio could be calculated for all positions by the statistic  $S_{\alpha,2}$ , given by:

$$\widehat{S}_{(\alpha,2)} = \sum_j \frac{F_j}{\sigma_j^2} \overleftarrow{T}_\alpha \widehat{P}_j \widehat{M}_j. \quad (21)$$

The test statistic that we are really interested in calculating for all positions is

$$\begin{aligned} S_{(0,1)} &= \ln(\mathcal{P}[M|\mathcal{H}_0]) - \ln(\mathcal{P}[M|\mathcal{H}_1]) \\ &= S_{(0,2)} - S_{(1,2)}. \end{aligned} \quad (22)$$

This is given by:

$$\begin{aligned} \widehat{S}_{(0,1)} &= \sum_j \frac{F_j}{\sigma_j^2} (\overleftarrow{T}_0 - \overleftarrow{T}_1) \widehat{P}_j \widehat{M}_j \\ &= (\overleftarrow{T}_0 - \overleftarrow{T}_1) \sum_j \frac{F_j}{\sigma_j^2} \widehat{P}_j \widehat{M}_j \\ &= (\overleftarrow{T}_0 - \overleftarrow{T}_1) \widehat{S}. \end{aligned} \quad (23)$$

This shows that using  $\widehat{S}$  (defined in Eq. 6) alone we can calculate the same numerical value for the log likelihood ratio as if we had all the images. This makes it clear that all the information needed in order to make a statistical decision is cast into  $S$ .

In order to perform the hypothesis testing all that remains is to specify the decision boundary. For that we need to calculate the expectancy and variance of  $S_{(0,1)}$  given both hypotheses. Using Equations 6,10, 16 and 17, we can calculate the expectancy of  $\widehat{S}$  given  $\mathcal{H}_\alpha$ , which is given by:

$$E[\widehat{S}|\mathcal{H}_\alpha] = \overleftarrow{T}_\alpha \sum_j \frac{F_j^2}{\sigma_j^2} |\widehat{P}_j|^2 = \overleftarrow{T}_\alpha F_R^2 |\widehat{P}_R|^2. \quad (24)$$

Similarly,

$$E[\widehat{S}_{(0,1)}|\mathcal{H}_\alpha] = T_\alpha (\overleftarrow{T}_0 - \overleftarrow{T}_1) F_R^2 |\widehat{P}_R|^2. \quad (25)$$

To calculate the variance of  $S_{(0,1)}$ , we first need its description in the image plane, which is (from Eq. 23):

$$S_{(0,1)} = (\overleftarrow{T}_0 - \overleftarrow{T}_1) \otimes \left( \sum_j \frac{F_j}{\sigma_j^2} \overleftarrow{P}_j \otimes M_j \right) = (\overleftarrow{T}_0 - \overleftarrow{T}_1) \otimes S, \quad (26)$$

<sup>5</sup> The lemma of Neyman & Pearson (1933) states that for simple hypotheses testing the log-likelihood ratio test is the most powerful test.

and therefore, the variance of  $S_{(0,1)}$  is:

$$V[S_{(0,1)}] = \sum_j \sum_x \left( \frac{F_j}{\sigma_j^2} \overleftarrow{(T_0 - T_1)} \otimes P_j \right)^2 (x) V(M_j(x)). \quad (27)$$

Using the Parseval equality, and the fact that  $V[M_j] = \sigma_j^2$ , we get:

$$V[S_{(0,1)}] = \sum_j \sum_f \frac{F_j^2}{\sigma_j^2} \left| \overleftarrow{(\widehat{T}_0 - \widehat{T}_1)} \widehat{P}_j \right|^2. \quad (28)$$

Noticing that  $F_R^2 |\widehat{P}_R|^2 = \sum_j \frac{F_j^2}{\sigma_j^2} |\widehat{P}_j|^2$  (Eq. 10), and simplifying, we get:

$$V[S_{(0,1)}] = \sum_f |\widehat{T}_0 - \widehat{T}_1|^2 F_R^2 |\widehat{P}_R|^2. \quad (29)$$

This means that any decision between two simple generative hypotheses can be done directly on  $S$ . To correctly normalize and analyze the derived score, we also need to store  $F_R^2 |\widehat{P}_R(f)|^2$ . This means that  $S$ ,  $P_R$  and  $F_R$ , or equivalently,  $R$ ,  $P_R$ , and  $F_R$  are sufficient for hypothesis testing on background-dominated noise images.

Moreover, by using  $R$ ,  $P_R$  and  $F_R$ , we notice that the hypothesis testing process is exactly the same as if  $R$  was a single image,  $P_R$  its PSF and  $F_R$  its transparency. To see this, we can further develop

$$S_{(0,1)} = R \otimes \left( F_R \overleftarrow{P}_R \otimes \overleftarrow{(T_0 - T_1)} \right), \quad (30)$$

which is the exact expression for simple hypothesis testing on the single image  $R$  with the PSF  $P_R$  and transparency  $F_R$ .

Testing composite hypotheses, which are hypotheses that have intrinsic parameters (an example problem is the star-galaxy separation task in which each hypothesis has a different set of parameters) requires a much more elaborate statistical process, on which there is no widespread agreement among statisticians. However, in the next subsection, we show that the set  $\{R, P_R, F_R\}$  is a sufficient statistic for all generative statistical models with constant image  $T$ . We do this by showing that any likelihood evaluation of every constant image  $T$  can be done using only  $\{R, P_R, F_R\}$ . Therefore any decision between any two statistical models, even composite models, can be done using  $\{R, P_R, F_R\}$  alone.

### 5.2. $\{R, P_R, F_R\}$ are sufficient for any measurement

Assuming we want to measure some parameters  $\theta$  of a generative model of the true image  $T$  (e.g., flux measurement of a star or fitting a galaxy model). Having a generative model means that each value of  $\theta$  predicts some  $T_\theta$ . The measurement process, whether Bayesian or frequentist, relies only on the calculation of the log-likelihood function  $\mathcal{L}(\theta)$  for all values of  $\theta$ . In order to show that  $\{R, P_R, F_R\}$  are sufficient, we will first show that the exact numerical value (of the part that depends on  $\theta$ ) of any likelihood evaluation of the data, given some true image  $T_\theta$  can be computed by using only  $\{R, P_R, F_R\}$ .

Following this, we prove that  $\{R, P_R, F_R\}$  are sufficient for any measurement of a constant in time property, using the Fisher-Neyman factorization theorem (Fisher 1922; Neyman 1935). This theorem states that a function  $\mathcal{F}$  of the data  $M$ , is

sufficient for  $\theta$  if and only if it satisfies that the log-likelihood  $\mathcal{L}$  of the data given  $\theta$  factorizes into:

$$\mathcal{L}(M|\theta) = f(M) + g_\theta(\mathcal{F}(M)), \quad (31)$$

where  $f$  is an arbitrary function that its argument is independent from the model parameters and  $g_\theta$  is an arbitrary function that depends on the data only thorough the statistic  $\mathcal{F}$ . We are going to show this for any generative model parametrized by  $\theta$  for the constant in time true image  $T(\theta)$ , and by that, show that  $\{R, P_R, F_R\}$  are sufficient for *any* time invariant measurement on the data.

The log of the probability to measure the data given a value of  $\theta$  for the generative model is (using the assumption of additive white Gaussian noise):

$$\mathcal{L}(M|\theta) = \sum_j \ln(\mathcal{P}(M_j|\theta)) \quad (32)$$

$$= \sum_j \sum_x \frac{|M_j(x) - (F_j T_\theta \otimes P_j)(x)|^2}{2\sigma_j^2}. \quad (33)$$

Using the Parseval equality, we can express the likelihood as a function of  $\theta$  by:

$$\mathcal{L}(M|\theta) = \sum_j \sum_f \frac{|\widehat{M}_j(f) - (F_j \widehat{T}_\theta \widehat{P}_j)(f)|^2}{2\sigma_j^2}. \quad (34)$$

Opening the squares, and keeping only terms that depend on  $\theta$  we get:

$$\begin{aligned} \mathcal{L}(\theta) &= \sum_f |\widehat{T}_\theta(f)|^2 \left( \sum_j \frac{|F_j \widehat{P}_j(f)|^2}{2\sigma_j^2} \right) - 2\Re \left[ \sum_f \widehat{T}_\theta \sum_j \widehat{M}_j \frac{F_j \widehat{P}_j}{2\sigma_j^2} \right] \\ &= \frac{1}{2} \sum_f \left( |\widehat{T}_\theta|^2 F_R^2 |\widehat{P}_R|^2 \right) (f) - \Re \left[ \sum_f \left( \widehat{T}_\theta \widehat{S} \right) (f) \right], \end{aligned} \quad (35)$$

where  $\Re$  denotes the real part operator. Furthermore, by adding the constant term  $\sum_f |\widehat{R}|^2$ , that does not depend on  $\theta$ , we can further simplify this to (using Eq. 15):

$$\begin{aligned} \mathcal{L}(M|\theta) + f(M) &= \sum_f \left( |\widehat{R}|^2 + |\widehat{T}_\theta|^2 F_R^2 |\widehat{P}_R|^2 - 2\Re \left[ \widehat{T}_\theta F_R \widehat{P}_R \widehat{R} \right] \right) \\ &= \sum_f \left| \widehat{R} - F_R \widehat{P}_R \widehat{T}_\theta \right|^2. \end{aligned} \quad (36)$$

Using the Parseval equality again, we get:

$$\mathcal{L}(M|\theta) = \sum_x \frac{(R - F_R P_R \otimes T_\theta)^2}{\sigma_R^2}. \quad (37)$$

The fact that the expression we derived depends on the data only through  $\{R, P_R, F_R\}$  proves, using the Fisher-Neyman factorization theorem that they are indeed sufficient for measuring the parameters of any generative model.

From examining Equation 37, we can see another important property of  $\{R, P_R, F_R\}$ , which is that the measurement process using them is *exactly* the same as if  $R$  was a regular single image,  $P_R$  its PSF and  $F_R$  is its transparency. This

means that performing measurements on  $\{R, P_R, F_R\}$  is indistinguishable from performing measurements on regular observations. Therefore any existing code that receives a single image could be used unchanged on  $R$ , getting  $P_R$  as the relevant PSF. This is the main reason why we prefer the set  $\{R, P_R, F_R\}$  over  $\{S, P_R, F_R\}$  even though they are statistically equivalent. There is another reason, which is the same reason why astronomers usually use images, and not matched-filtered images – they are more intuitive to interpret.

## 6. EXAMPLES

In §5 we presented major advantages of proper image coaddition. These are optimal  $S/N$ , and the ability to perform any measurement or decision optimally without the original images. Another advantage of this method, as we mentioned earlier, is that it has a PSF which is typically sharper than the sharpest image in the original set. In order to demonstrate these advantages of the new method over the popular methods we present here a few simulated examples (§6.1) as well as coaddition of real seeing-limited data (§6.2) and speckle images (§6.3). Additional examples, more specific to fast imaging applications, with a much more quantitative analysis, will be presented in future papers of this series.

### 6.1. Visualization of the $R, P_R$ statistics for various special cases

Here we show visual examples of the results of the coaddition process, performed on simulated data. We directly compare these results to the naive direct sum of images. In order to differentiate the effect of the PSF shape from that of the transparency and background, we use equal transparency ( $F_j$ ) and background variance ( $B_j$ ) for all images coadded. We note that under these conditions even the more elaborate weighted addition methods (Annis et al. 2014; Jiang et al. 2014) boil down to a direct sum. Figure 1 compares the PSFs of the direct sum with that of the proper image (Eq. 10), while Figure 2 shows the resulting differences in the images of a point source, with noise, between the direct sum and proper coaddition (Eq. 7). Figure 3 shows the same as Figure 2 but for a binary star with a separation of 10 pixels and 1 magnitude flux difference. Each row in Figure 1 shows, left to right, four PSFs (denoted  $P_1$  to  $P_4$ ), the PSF resulting from simple coaddition ( $\frac{\sum_j P_j}{N_{\text{im}}}$ ), where  $N_{\text{im}}$  is the number of images coadded, and the PSF of the proper image ( $P_R$ ; right column). The first row corresponds to Gaussian PSFs with varying widths (i.e., varying standard deviations), where the Gaussian standard deviations are 8, 10, 15 and 18 pixels, respectively. The second row shows highly elliptical PSFs with varying orientations, while the third row shows speckle images of a point source, simulated with  $D/r_0 = 10$ , where  $D$  is the telescope diameter and  $r_0$  is the Fried length (Fried 1966). Apart from the visually better PSF, properly coadding images results in lower noise standard deviation relative to other methods. This effect can be seen in Figures 2 and 3. In these figures, we compare naive coaddition ( $\sum_j M_j$ ) and the proper image ( $R$ ) of noisy simulated images with PSFs chosen as in Figure 1, both normalized to have a noise standard deviation of 1 and are shown with the same gray scale. It is clearly seen that both the shape and the signal to noise of the images are better in the properly coadded image than in the naive summation of the images.

To aid comparison, we plot the central horizontal cuts through all coadd images presented in Figures 1, 2 and 3 in Figures 4, 5 and 6, respectively. The gray lines show the re-

sult of simple coaddition, while the black lines show the result of proper coaddition.

We note that our coaddition technique is optimal by construction, and is not assuming anything on the images themselves (except having background dominated, uncorrelated Gaussian noise). Therefore, it works optimally on any complex image. An example for this is given in Figure 6, in which the input image was a simulated binary star. It is very clear that the 1 magnitude fainter companion can be easily detected by further signal processing of the proper image in both the asymmetric PSF case (second row) and speckle PSF case (third row).

The coaddition method we present will provide the largest improvement in comparison to weighted coaddition when there is a large diversity in the PSF shape between the coadded images. In our examples, the most prominent effect is seen in the case of the speckle images. It is further striking, that the proper coaddition of speckle images generates an image containing substantial spatial information right to the diffraction limit (see demonstration on real images in §6). Given the importance of this subject we discuss this in detail, under different scientifically relevant observational situations, in future papers.

### 6.2. Tests on real seeing-limited observations

For source detection, the method we present in this paper is identical to the technique outlined in paper I. The reason for this is that in order to find sources in our optimal coadd image (Eq. 7), we need to cross correlate the image with its PSF (Eq. 10). Doing this will result in Equation 5 which is simply the method we presented in paper I. Nevertheless, in practice numerical errors, and sub-optimal estimation of the various properties (e.g., PSF) may slightly change the outcome. Therefore, it is important to demonstrate that in practice the method presented here returns the same results as the optimal coaddition for source detection in paper I, and that these results are better than those obtained using other techniques.

As in paper I, we test our method on data from the Palomar Transient Factory (PTF; Law et al. 2009; Rau et al. 2009) Data Release 2. The image reduction process is described in Laher et al. (2014), and photometric calibration is discussed in Ofek et al. (2012). Furthermore, we use the same datasets and tools as before. We used four datasets, and for each dataset we constructed a deep reference image, from over 400 good seeing images, coadded using the Annis et al. (2014) method. Next, for each dataset we choose small subsets, containing 19 to 45 random-seeing images, and coadded these images using various methods including equal weights, Annis et al. (2014) weighted coaddition, Jiang et al. (2014) coaddition and our proper coaddition technique. The selection criteria for each data set are listed in Table 1. For more details we refer the reader to paper I.

We note that there are two ways to calculate the PSF of the proper coaddition image. The first is to measure it from the proper coaddition image, while the second is to calculate it using Equation 7, and the PSFs measured in the individual images. Using the test data presented in paper I, we find that the second method gives much better results than the first method. This is likely due to the way that errors are propagated in the two schemes, and means that storing  $P_R$  is recommended.

We ran several tests on the various coadd images. We ran our source extraction code (see paper I for details) on the various images, and matched the sources against those found in the deep reference image. This allowed us to quantify how

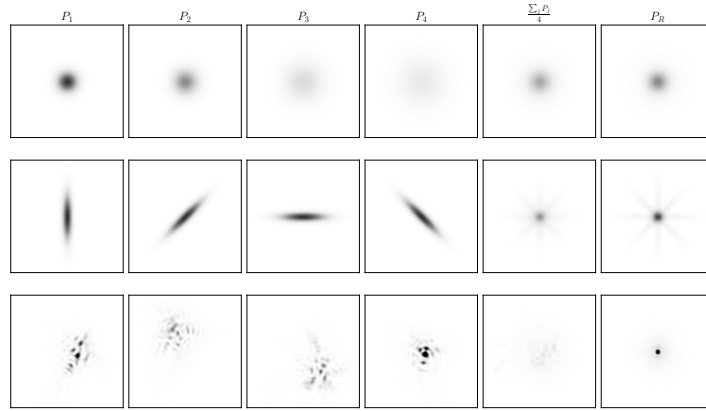


**Figure 1.** An image illustrating the point spread functions (PSF) of properly added images. The four left columns: Individual simulated PSFs. Second from the right: Regular equal weights coaddition. Right: The PSF of the proper coaddition image (i.e., using Eq. 10). On top: Gaussian PSFs with widths of 8, 10, 15 and 18 pixels respectively. Middle: PSFs are elliptical Gaussians with various orientations and a width of 5 pixels and 25 pixels on the short and long axes, respectively. Bottom: simulated speckle PSFs, corresponding to  $\frac{D}{r_0} = 10$ , where  $D$  is the telescope diameter and  $r_0$  is the Fried length. In the case of speckle images, 20 images were coadded, but only 4 of the original images are displayed. Coadded images on the same row are displayed with the same color map.

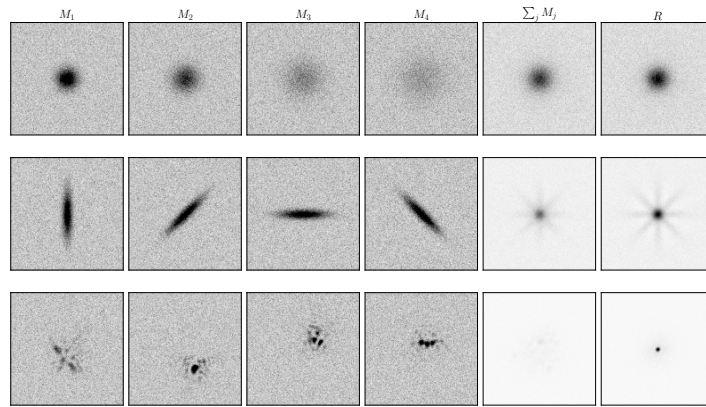


**Figure 2.** Like Fig. 1, but showing the images, with noise, rather than the PSFs (i.e., using Eq. 7). Coadd images are shown in the same gray scale, and are normalized to have the same noise standard deviation.

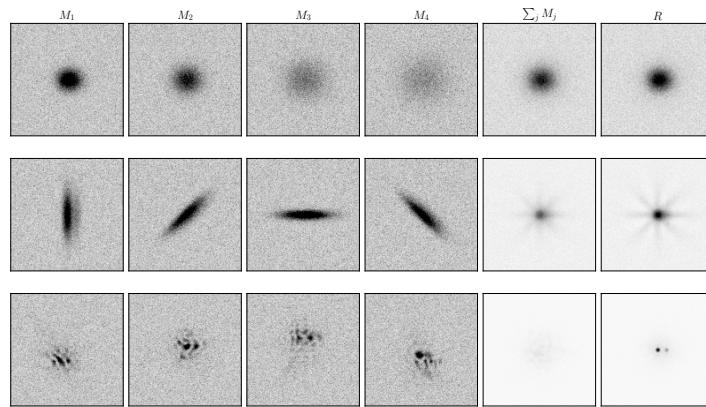


**Figure 3.** Same as Fig. 2, but where the source is a binary star with separation of 10 pixels and flux ratio of 2.5.

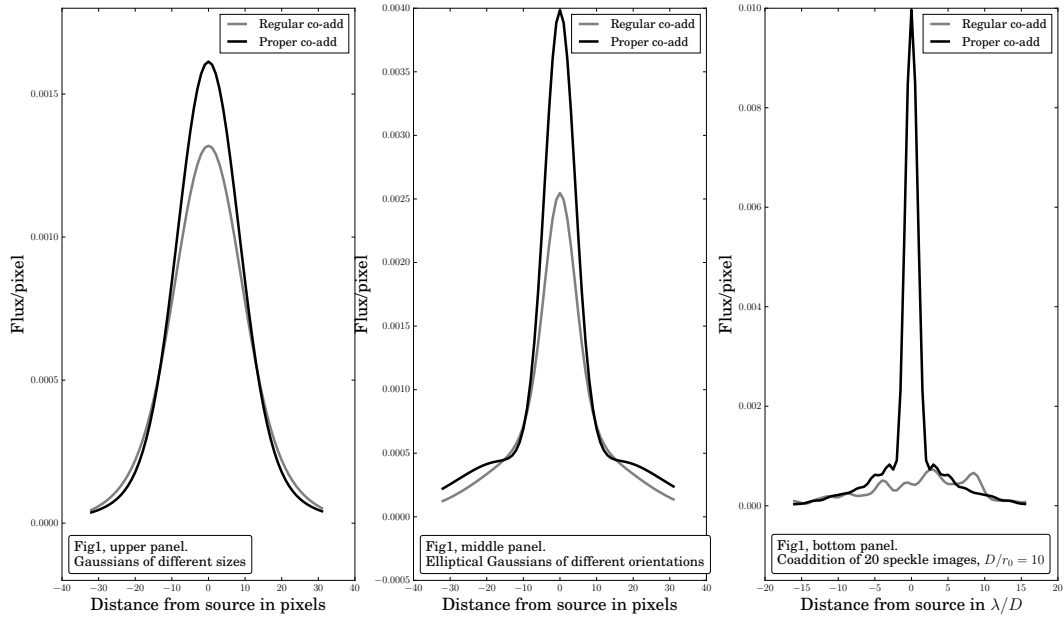


**Figure 4.** Intensity values of the point spread functions presented in Figure 1 along a line crossing at its center. Black – The PSF of the properly added images. Grey: – The PSF of the regularly summed images. Left: cross cuts for the top row (circular Gaussians of different widths). Middle: cross cuts for the middle row (elliptical Gaussian PSFs with various orientations). Right: cross cuts for the bottom row (speckle images).

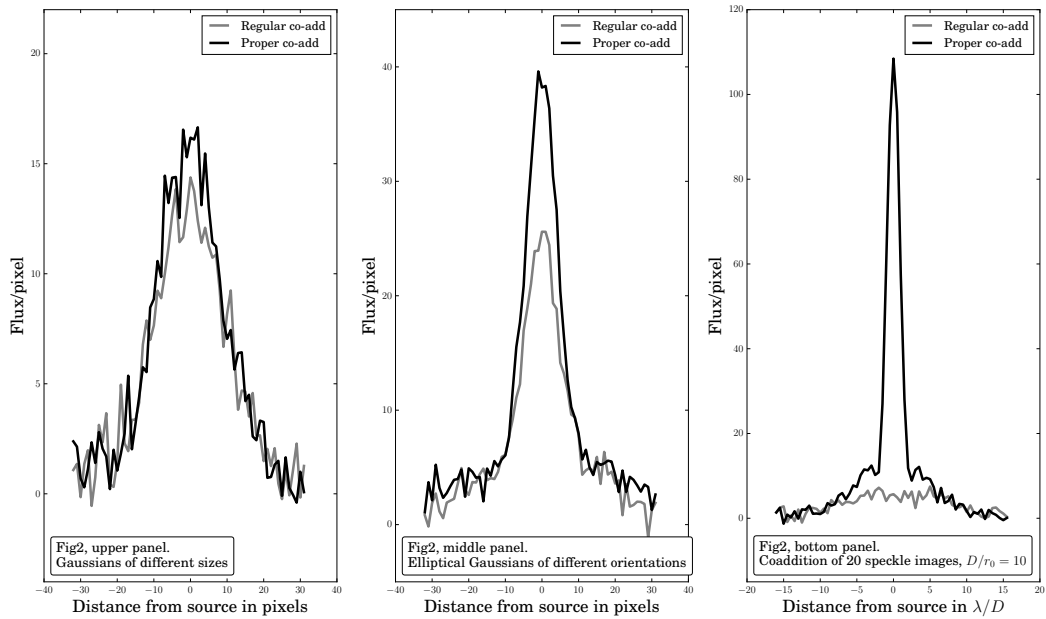


**Figure 5.** Like Fig. 4, but corresponding to the images presented in Figure 2.

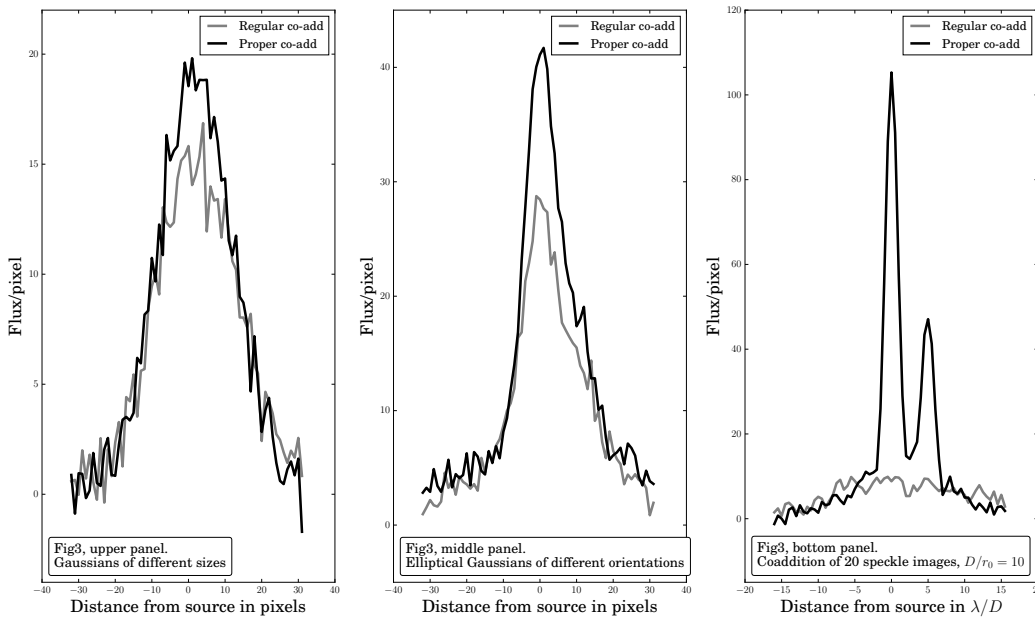


Figure 6. Like Fig. 4, but corresponding to the images presented in Figure 3.

Table 1  
Sets of images used in the comparison

Set	Field	CCD	#im	Type	Criteria
1	100031	6	425	Ref.	Variance < 1000 e <sup>-</sup> & FWHM < 4" & > 10 PSF stars
			45	coadd	All images taken on Oct, Nov, Dec 2012 & > 10 PSF stars
2	100031	6	425	Ref.	Variance < 1000 e <sup>-</sup> & FWHM < 4" & > 10 PSF stars
			48	coadd	All images taken on the first 9 days of each Month in 2011 & > 10 PSF stars
3	100031	4	263	Ref.	Variance < 1000 e <sup>-</sup> & FWHM < 4" & > 10 PSF stars
			39	coadd	All images taken on Oct, Nov, Dec 2012 & > 10 PSF stars
4	100031	4	263	Ref.	Variance < 1000 e <sup>-</sup> & FWHM < 4" & > 10 PSF stars
			17	coadd	All images taken on the first 9 days of each Month in 2011 & > 10 PSF stars

**Note.** — Selection criteria for reference images and coadd images in the various sets used for testing the coaddition methods. Field indicate the PTF field ID, while CCDID is the CCD number in the mosaic (see Law et al. 2009; Laher et al. 2014). Type is either Ref. for the deep reference image, or Coadd for the subset we coadd using the various methods. Note that field 100031 is in the vicinity of M51. This table is identical to Table 1 in paper I.

many real stars and how many false detections are reported based on each coaddition method. The number of real sources and false sources found in each image in each dataset is given in Table 2.

Furthermore, like in paper I, we compared the detection  $(S/N)^2$  (proportional to the survey speed and information content) of the sources in the various images. For each star detected in the reference image we divide its  $S/N$  measured in a coaddition image by its  $S/N$  measured in our properly coadded image. Next we take the median of the squares of these ratios. This roughly gives the survey speed of each coadded image, relative to our coaddition method, and is listed in Table 2 ( $I_r$ ).

Table 2 indicates that our proper coaddition method returns the same results, up to some small numerical differences, as the optimal coaddition for source detection presented in paper I. Next it is clear that our method perform better than the other popular methods.

Another important point is that the effective PSF of our

method is typically sharper than the PSF of other methods. Figure 7 shows an example of a cut through the PSFs of various image coaddition techniques (using dataset 3). The proper image coaddition (black line) has narrower and higher PSF than other methods. This demonstrates, as shown in §4 and §5, that the proper image indeed contains more spatial information than existing methods, and provides significant improvement to the quality of all further signal processing of the coadd image, both in theory and in practice. To summarize, the method presented in this paper, provide a few percents to 25% improvement in terms of survey speed (or information content) over popular weighted coaddition techniques (e.g., Annis et al. 2014; Jiang et al. 2014; see paper I for details). Furthermore, the effective PSF of the coadded images is typically sharper than those provided by popular image coaddition methods.

### 6.3. Tests on real speckle images

**Table 2**  
Comparison between coaddition methods

Set	Method	$I_r$	$N_d$	$N_r$	$N_u$	$N_f$
1	Deep	0	2433	...	...	...
	Equal weights	0.65	1136	1087	1346	49
	Annis et al. (2014)	0.91	1332	1255	1178	77
	Jiang et al. (2014)	0.89	1299	1229	1204	70
	paper I	1	1417	1324	1109	93
2	Deep	0	2433	...	...	...
	Equal weights	0.59	1183	1085	1348	98
	Annis et al. (2014)	0.93	1481	1343	1090	138
	Jiang et al. (2014)	0.90	1421	1301	1132	120
	paper I	1	1541	1390	1043	151
3	Deep	0	4062	...	...	...
	Equal weights	0.53	1645	1539	2523	106
	Annis et al. (2014)	0.84	1955	1796	2266	159
	Jiang et al. (2014)	0.81	1912	1759	2303	153
	paper I	1	2206	1976	2086	230
4	Deep	0	4062	...	...	...
	Equal weights	0.83	2319	2007	2055	312
	Annis et al. (2014)	0.82	2144	1981	2081	163
	Jiang et al. (2014)	0.92	2272	2062	2000	210
	paper I	1	2401	2125	1937	276
This work	0.99	2400	2124	1938	276	276

**Note.** — Quantitative comparison between images coadded using various technique matched against a deep reference image. The four blocks, separated by horizontal lines, correspond to the four data sets in Table 1.  $I_r$  is the approximate survey speed ratio between the image compared and our optimal coaddition method (see text for details).  $N_d$  is the number of detected sources to detection threshold of  $4\sigma$ .  $N_r$  is the number of real sources (i.e., detected sources which have a counterpart within  $3''$  in the deep reference image).  $N_u$  is the number of real undetected sources (i.e., sources detected in the reference which are not detected in the coadd image).  $N_f = N_d - N_r$  is the number of false detections. This table is identical to Table 2 in paper I.

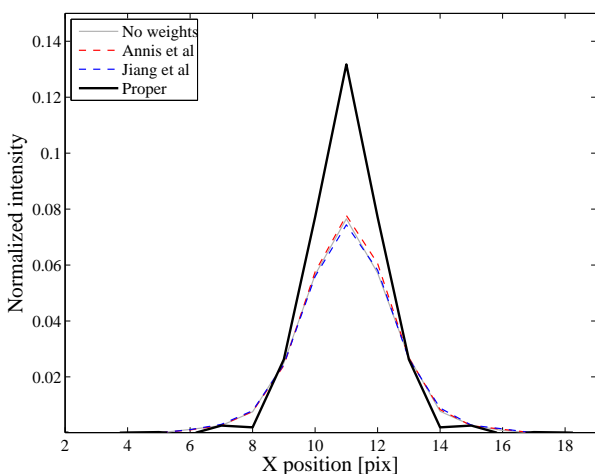


**Figure 7.** A cut through the PSF of the various methods based on dataset 3 from paper I. Shown are the proper coaddition image (black line), the unweighted addition (gray line), Annis et al. (2014) weighted addition (dashed red line), and Jiang et al. (2014) weighted addition (dashed blue line). All the PSFs are normalized to have unity sum. The PSF of the proper coaddition was calculated using Equation 10.

As evident from the third row of Figures 1,2 and 3, proper image coaddition has a great potential for high resolution imaging. Unlike lucky imaging (Law et al. 2006) this method uses the best possible linear combination of *all* the images. Furthermore, unlike speckle interferometry (Labeyrie 1970) and deconvolution from wave-front sensing (DWFS; Primot et al. 1990), this method is numerically stable and does not invent non-existing information, or introduce long range correlations into the data. It is worth while to explain these two points. In the case of speckle interferometry, due to the division by small numbers in the Fourier space, the noise component in poorly known spatial frequencies is amplified, and becomes correlated noise in the real space. This noise limits the contrast of speckle interferometry as well as any honest significance analysis of detected companions. This is a major reason why astronomers resort to visual inspection of the auto-correlation maps produced by speckle interferometry for binary detection. Furthermore, because deconvolution methods enforce a delta function PSF for the images, they invent non-existing information about poorly known spatial frequencies (e.g., above the Nyquist frequency).

In future papers we will discuss our new de-speckling techniques. These techniques are based, with some modifications for source dominated noise and unknown PSF, on Equation 7.

The formula we derived in this paper is optimal only for the background-noise-dominated case, but it is worth while to visualize its performance as is for real images, even if they are source-noise dominated. Here we wish to briefly demonstrate that this method has an excellent potential for high contrast imaging via speckle observations, but for additional details, as well as new mathematical derivations, improvements and comparisons to existing methods, see future papers.

To test this we obtained 30000 7 ms images of the star COU 1049 (RA =  $00^h29^m45^s.34$ , Dec =  $+36^\circ50'23''.7$ ). The images were taken using the Kraar Observatory<sup>6</sup> 40cm telescope equipped with an Andor/Zyla sCMOS camera. The camera has  $6.5 \mu\text{m}$  pixels, and we observed using a Barlow lens, extending the focal ratio to  $f/25$ , so the pixel scale was  $0.13'' \text{pix}^{-1}$ . This pixel scale is smaller than the Nyquist frequency of the optics, allowing for diffraction limited resolution if the best possible correction is applied. We note that this is not an essential requirement for the application of the method. The images were taken under seeing conditions of  $1.2''$ - $1.5''$  full width half max. This is equivalent to  $D/r_0 \approx 5$ , where  $D$  is the telescope aperture and  $r_0$  is the Fried length (Fried 1966). Figure 8 presents the coadd image using Equation 7. As the PSF, we used the image itself. COU1049 is a binary star system, with separation of  $0.7''$ . Its primary and secondary magnitudes are 9.8 and 10.15, respectively. The de-speckled image created by proper coaddition clearly shows the companion, along with its mirror image. This mirror image is generated due to the fact we used the image as its own PSF. Figure 9 shows a cut through the PSFs of the two components. First it is evident that the proper coaddition of speckle images reveals diffraction limited information. Quantitative and qualitative comparison of this method to existing speckle imaging methods are left to future papers.

## 7. CODE AND IMPLEMENTATION DETAILS

The code we use to implement the proper image coaddition is similar to the code presented in paper I. The only additional program required is the MATLAB function

<sup>6</sup> <http://www.weizmann.ac.il/particle/kraar/home>

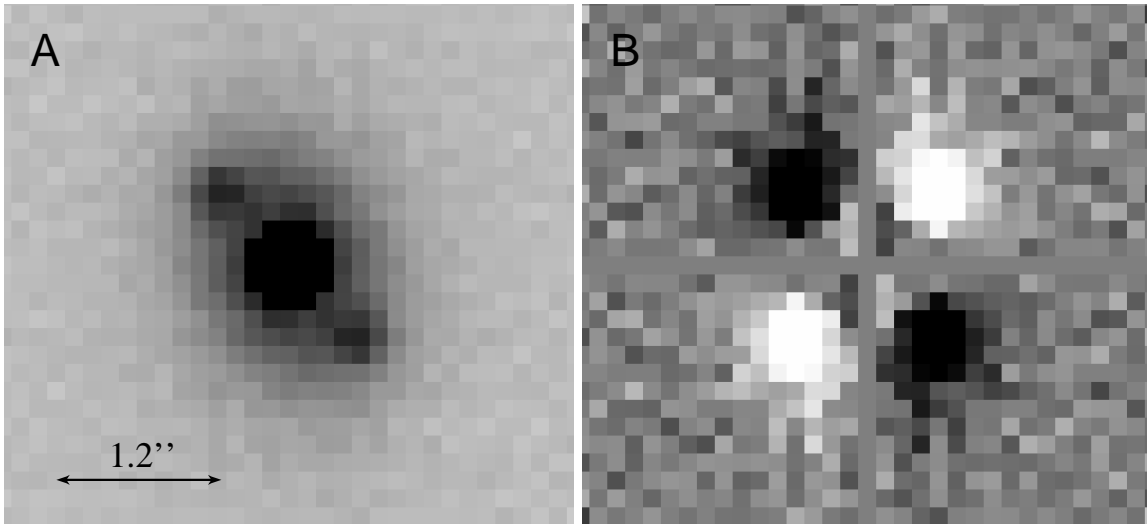


**Figure 8.** **Panel A:** A proper coaddition of 30,000 7 ms exposures (speckle images) of the binary star COU1049. The images were taken under seeing of  $1.2''$ - $1.5''$  FWHM. The companion, at angular distance of  $0.75'' \pm 0.1''$  is clearly detected, along with its mirror image. The mirror image is generated due to the fact that we used the image as its own PSF. The FWHM of the resulting image is about  $0.35''$  (note that it is comparable to the diffraction limit;  $\lambda/D \cong 0.3''$ ). **Panel B:** A symmetric subtraction of the coadded image with respect to the central vertical axis. The PSF is expected to be symmetric, therefore this removes the primary star's contribution. We are left with two positive and two negative copies of the companion.

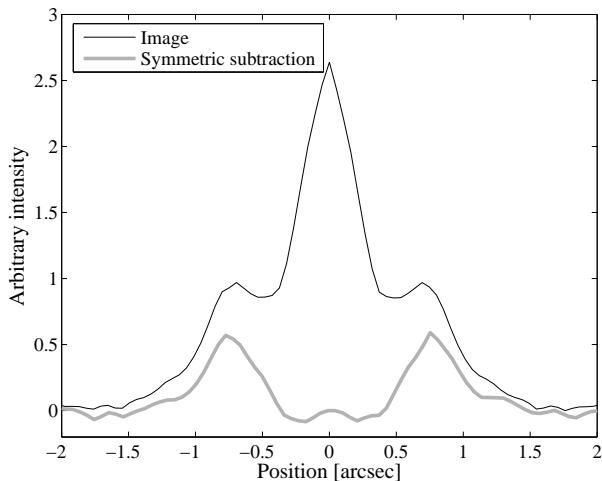


**Figure 9.** A cut through the COU1049 star and its companion shown in Figure 8. Black line is for Panel A while the gray line is for Panel B. The achieved seeing FWHM is  $0.35''$  (see Fig. 8 for details), which is substantially smaller than the  $1.2''$ - $1.5''$  FWHM in the original images.

`sim_coadd_proper.m`. This function gets the images (optionally not aligned), their weights and PSFs, and returns the proper coadded image and its PSF, where the PSF is calculated using Equation 10, rather than measuring it from the proper coadd image. All the calibration steps (registration and PSF, background, and variance estimation) were done using the same programs described in paper I. All the code is available as part of the MATLAB astronomy and astrophysics package<sup>7</sup> (Ofek 2014).

We note that the usual implementation problems like registering the images, resampling them to the same grid, measuring the background and variance levels, and measuring/interpolating the PSF, as always, require attention. However, the attention to the details given this method is not different than in the case of other methods. Nevertheless, we suggest that care will be given to the following points:

**Taking care of defects in the images:** It is important to note that this method is not generalized yet to use robust estimators like median or sigma clipping (see discussion in paper I). Therefore, one needs to take care of image artifacts (bad pixels, cosmic rays, ghosts) prior to the coaddition process. We recommend on detecting these artifacts prior to the coaddition, and interpolating over the bad pixels. This can be done using existing algorithms like van Dokkum (2001); Ipatov et al. (2007); Ritter et al. (2014). Alternatively, cosmic ray removal can be done using image subtraction. However, this requires a sensitive image subtraction method which is free of subtraction artifacts, and that has predictive and small effects on the shape and contrast of delta function events. Such a method is demonstrated in Zackay, Ofek & Gal-Yam (2015).

The following additional points were also discussed in paper I:

**background and variance estimation:** The background and variance in real wide-field-of-view astronomical images cannot be treated as constants over the entire field of view. Therefore, we suggest to estimate them locally and interpolate. To estimate the background and variance one needs to make sure that the estimators are not biased by stars or small galaxies. Our suggestion is to fit a Gaussian to the histogram of the image pixels in small regions<sup>8</sup>, and to reject from the fitting process pixels with high values (e.g., the upper 10% of pixel values).

**Estimating the transparency:** The transparency  $F_j$  of each image is simply its flux-based photometric zero point. However, one has to make sure that this zero point is measured using PSF photometry rather than aperture photometry, otherwise the zero point may depend also on the seeing.

**Estimating the PSF:** Among the complications that may affect the PSF measurement are pixelization and interpolation and the resampling grid. Furthermore, the PSF is likely not constant spatially and it also may change with intensity due to charge self repulsion. This specifically may lead to the brighter-fatter effect (e.g., Walter 2015). We note that the fact

<sup>7</sup> <http://webhome.weizmann.ac.il/home/eofek/matlab/>

<sup>8</sup> We are currently using  $256 \times 256$  arcsec<sup>2</sup> blocks.

that one needs to estimate the PSF in order to run this method should not be viewed as a drawback, as any decent method that finds sources in the image requires this step anyway.

#### 8. SUMMARY

We present a coaddition method which has the following properties:

- It is optimal for the background-noise-dominated case.
- If the input images have equal variance and uncorrelated noise, then the output image has equal variance and uncorrelated noise.
- It provides maximum  $S/N$  measurement of the constant sky image on all spatial frequencies.
- It is a sufficient statistic for any hypothesis testing or measurement, and hence represents all the constant-in-time information in the data.
- Its PSF is typically as sharp or sharper than the PSF of the sharpest image in the ensemble.
- It is trivial to program and since it involves only FFT and simple operators, it is also fast to compute.
- Unlike deconvolution or some PSF homogenization techniques, it is numerically stable.
- It provides excellent results for separating binary stars to the diffraction limit in speckle images.
- It applies only local operations on the input images (i.e., convolution with a finite-size PSF). Therefore it allows one to use a slowly-varying position-dependent PSF.

The method can be summarized using two simple equations. Equation 7 describes the image coaddition process, while Equation 10 provides the PSF of the coadd image. This method may have far-reaching implications for several fields. In Figures 1 through 6 we show how well this methods works on speckle images, and we further discuss this in detail in future papers.

For seeing-limited surveys like PTF and LSST this method may provide an increase of a few percent to 25% in the survey speed, compared with popular methods (e.g., Annis et al. 2014). The exact improvement depends on the seeing, background, and transparency distributions.

In addition, it will significantly reduce the need for data access, as all multi-epoch data gathered in the survey could be reduced to a single image, and its PSF, in every sky location. Moreover, the images themselves will be easier to process (both in terms of processing speed and memory requirements) because only one image will be needed to be dealt with, instead of many images of the same field (which could amount to thousands of images).

Another example is the potential of this method for weak lensing studies, that require shape measurements. An ideal shape measurement on an ensemble of images is to convolve the model with each of the individual image PSFs, and simultaneously fit the model to all images with the appropriate weights. This is a complicated process and as far as we know this is not commonly done. We showed that fitting a model to our coadd image and using its PSF is equivalent to doing the simultaneous fit on all the images and thus, it is an enabling technique for weak lensing.

We thank Avishay Gal-Yam, Guy Nir, Ora Zackay, Maayane Soumagnac, Adam Rubin, Frank Masci, Dovi Poznanski and Assaf Horesh for their comments and suggestions. We thank Guy Nir and Ilan Manulis for help with obtaining the speckle images presented here. B.Z. is grateful for receiving the Clore fellowship. E.O.O. is incumbent of the Arye Dissentshik career development chair and is grateful for support by grants from the Willner Family Leadership Institute Ilan Gluzman (Secaucus NJ), Israel Science Foundation, Minerva, Weizmann-UK, and the I-Core program by the Israeli Committee for Planning and Budgeting and the Israel Science Foundation (ISF).

#### REFERENCES

- Annis, J., Soares-Santos, M., Strauss, M. A., et al. 2014, *ApJ*, 794, 120  
 Fisher, R.A. (1922) *Philos. Trans. Roy. Soc. series A*, 222:309-368.  
 Fried, D. L. 1966, *Journal of the Optical Society of America* (1917-1983), 56, 1372  
 Hoekstra, H., Mellier, Y., van Waerbeke, L., et al. 2006, *ApJ*, 647, 116  
 Homrighausen, D., Genovese, C. R., Connolly, A. J., Becker, A. C., & Owen, R. 2011, *PASP*, 123, 1117  
 Ipatov, S. I., A'Hearn, M. F., & Klaasen, K. P. 2007, *Advances in Space Research*, 40, 160  
 Ivezić, Z., Tyson, J. A., Abel, B., et al. 2008, *arXiv:0805.2366*  
 Jiang, L., Fan, X., Bian, F., et al. 2014, *ApJS*, 213, 12  
 Kaiser, N., Aussen, H., Burke, B. E., et al. 2002, *Proc. SPIE*, 4836, 154  
 Keller, S. C., Schmidt, B. P., Bessell, M. S., et al. 2007, *PASA*, 24, 1  
 Labeyrie, A. 1970, *A&A*, 6, 85  
 Laher, R. R., Surace, J., Grillmair, C. J., et al. 2014, *PASP*, 126, 674  
 Law, N. M., Mackay, C. D., & Baldwin, J. E. 2006, *A&A*, 446, 739  
 Law, N. M., Kulkarni, S. R., Dekany, R. G., et al. 2009, *PASP*, 121, 1395  
 Neyman, J. (1935) *Giorn. Ist. Ital. Att.*, 6:320-334.  
 Neyman, J. & Pearson, E. S. 1933 *Philosophical Transactions of the Royal Society of London A: Mathematical, Physical and Engineering Sciences*  
 Ofek, E. O., Laher, R., Law, N., et al. 2012, *PASP*, 124, 62  
 Primot, J., Rousset, G., & Fontanella, J. C. 1990, *Journal of the Optical Society of America A*, 7, 1598  
 Rau, A., Kulkarni, S. R., Law, N. M., et al. 2009, *PASP*, 121, 1334  
 Ritter, A., Hyde, E. A., & Parker, Q. A. 2014, *PASP*, 126, 170  
 The Dark Energy Survey Collaboration 2005, *arXiv:astro-ph/0510346*  
 van Dokkum, P. G. 2001, *PASP*, 113, 1420  
 York, D. G., Adelman, J., Anderson, J. E., Jr., et al. 2000, *AJ*, 120, 1579  
 Zackay, B., & Ofek, E.O. 2015 submitted to *ApJ*  
 Zackay, B., Ofek, E.O. & Gal-Yam 2015 In preparation.